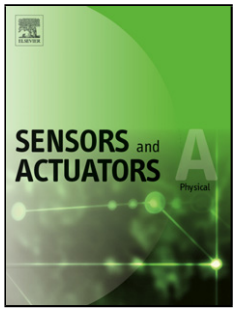

Orthogonal Optimal Design Method for Point-Focusing EMAT Considering Focal Area Dimensions

Hongyu Sun (Conceptualization) (Methodology) (Software) (Writing - original draft), Songling Huang (Supervision) (Project administration), Qing Wang (Visualization), Shen Wang (Validation), Wei Zhao (Resources) (Formal analysis)

PII: S0924-4247(19)31803-5

DOI: https://doi.org/10.1016/j.sna.2020.112109

Reference: SNA 112109

To appear in: *Sensors and Actuators: A. Physical*

Received Date: 30 September 2019

Revised Date: 3 May 2020

Accepted Date: 25 May 2020

Please cite this article as: Sun H, Huang S, Wang Q, Wang S, Zhao W, Orthogonal Optimal Design Method for Point-Focusing EMAT Considering Focal Area Dimensions, *Sensors and Actuators: A. Physical* (2020), doi: https://doi.org/10.1016/j.sna.2020.112109

Orthogonal Optimal Design Method for Point-Focusing EMAT Considering Focal Area Dimensions

Hongyu Sun[1], Songling Huang[1]*, Qing Wang[2], Shen Wang[1], Wei Zhao[1]

[1]*State Key Lab. of Power System, Department of Electrical Engineering, Tsinghua University, Beijing, 100084, China.*
[2]*Department of Engineering, Durham University, Durham, UK.*
* Correspondence to: Songling Huang. (E-mail: huangsling@tsinghua.edu.cn)

Graphical abstract

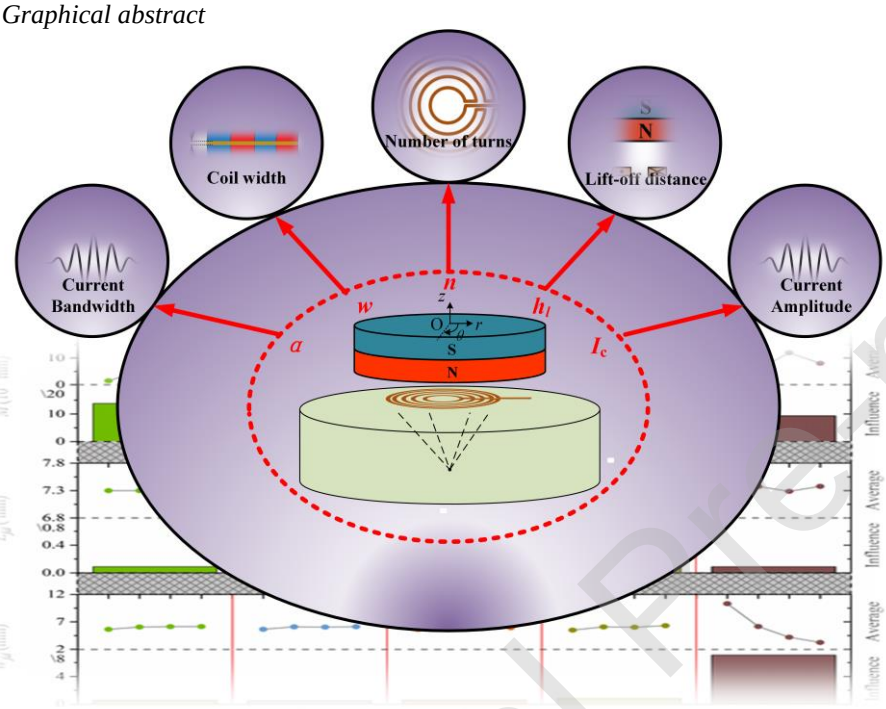

Highlights

- In this work, FEM simulation and orthogonal test methods are used to study the effect of impact factors on the PFSV-EMAT's performance. Five factors are selected in the test to investigate the signal intensity and focal area dimensions of the transducer. Range analysis is applied to compare the influence degree of each factor. In addition, drive frequency f and focal depth l_{Fz} are also studied individually. Considering the influence of different factors on different results, the optimal combination of parameters can be obtained. The effectiveness of the optimization method is verified by both simulation and experiment. Moreover, the experiments show that the focusing intensity of the optimized transducer is 400% higher than the average value of the non-optimized transducers, the effective focal length is reduced by 15%, and the effective focal width is reduced by 57%.

Abstract

Although ultrasonic focusing methods have been widely used in electromagnetic acoustic transducers (EMATs) to solve the problem of their low energy conversion efficiency, the influence of focusing accuracy on defect identification also warrants consideration. The dimension of the focal area that acts as an important factor and affects the detection accuracy has not been fully investigated recently to our knowledge. In this work, we report a parameter optimization method using an orthogonal test when considering the focusing intensity and focal area together. The results of the range analysis show that the factor lift-off distance h_l has the greatest impact on signal intensity M. Considering the dimensions of the focal area, bandwidth factor α has the largest effect on the effective focal length L_{fd}. For effective focal width W_{fd}, the concentric line source (CLS) number n has the largest

effect. Therefore, a smaller lift-off distance, larger CLS number, and suitable bandwidth factor α are required in a point-focusing SV EMAT (PFSV-EMAT). The optimal combination of parameters can be obtained by considering the influence of different factors on the results. The experiment shows that the signal intensity of the optimized transducer is nearly 400% higher than non-optimized ones and the effective focal length and width are reduced by 15% and 57%, respectively.

Key words: PFSV-EMAT; focal area dimensions; orthogonal test; optimal method; ultrasonic focusing

I. INTRODUCTION

Nondestructive testing (NDT) technology has been widely used in industrial fields as a method for detecting defects in a manner that does not damage the materials [1–4]. Ultrasonic wave detection, as an NDT technology, has the characteristics of rapid, long-distance detection and good environmental adaptability [5–9]. Ultrasonic wave detection technology based on the piezoelectric ultrasonic transducer is commonly used to detect metal plate defects [10–13]. This technology requires the use of a piezoelectric ultrasonic transducer to excite ultrasonic vibrations that are transmitted to the plate by a couplant, thereby realizing ultrasonic wave detection. However, detection technology based on the piezoelectric ultrasonic transducer needs to couple the ultrasonic vibrations into the metal plate by the couplant, so it is difficult to apply this to the detection under special working conditions such as noncontact requirements and high temperature [14, 15]. The electromagnetic acoustic transducer (EMAT) generates periodic Lorentz forces inside specimens via electromagnetic coupling, thereby exciting the ultrasonic wave [16, 17]. The bulk wave transducer uses EMAT to generate shear vertical (SV) body waves and is mainly used for defect detection in aluminum blocks. However, the EMAT has not been widely used, mainly because of its low energy conversion efficiency. Besides, air-coupled transducers have the advantage of noncontact and independence from the couplant. However, due to the excessive difference in acoustic impedance, the ultrasonic waves generated by this method are subject to severe energy attenuation, particularly when sound waves pass through the interface between the air and the metal [18, 19].

In electromagnetic ultrasonic bulk wave detection, the intensity of the SV waves is reduced due to the divergence of the beam direction, so the detection accuracy is then reduced. Therefore, line-focusing SV EMAT (LFSV-EMAT) was proposed by Ogi [20]. A sharp peak at the designed focal line was achieved in his work, which proves the coil design's effectiveness. However, this beam direction focusing method makes it difficult to achieve phase consistency, and a high signal focusing intensity cannot be obtained. Then, Ogi improved the LFSV-EMAT and he found that excited SV waves successfully became coherent on a focal line after traveling along oblique paths [21]. However, this method could only achieve a 2D line focusing on the SV waves and could not achieve 3D point focusing, so it was difficult to determine the spatial shape and size of the defect. Then, the point-focusing method was proposed by Takishita, and he utilized curved meander line (CML) coils to focus the SV waves on a certain point within the space [22]. The detection accuracy and signal resolution of the SV waves were further improved by using point-focusing SV EMAT (PFSV-EMAT). However, the effect of transducer parameters on the PFSV-EMAT focusing performance was not considered here, nor in other studies [23, 24]. To solve this problem, Jia used the orthogonal test method to investigate the focusing performance for a PFSV-EMAT and analyzed the effects of various parameters on the focal intensity and focal offset of the transducer [25]. However, the size of the focal area greatly influences the defect detection accuracy, and the smaller focal size can improve the imaging resolution and concentrate the sound energy effectively.

Therefore, this work utilizes the orthogonal test method to study the effect of each factor on the PFSV-EMAT's focusing performance. The signal intensity M, the effective focal length L_{fd}, and the width W_{fd} (focal area dimensions) are considered in the test. Seven factors are selected: The coil width w, the lift-off distance h_l, the excitation current amplitude I_c, the bandwidth factor α, the line source number n, the drive frequency f, and the focal depth l_{Fz}. Since changing f and l_{Fz} will cause a change in the coil structure, only the other five factors are selected in the orthogonal test and the orthogonal table $L_{16}(4^5)$ is used here. The Finite Element Method (FEM) is used to calculate the required results and the optimized parameter combination is obtained through range analysis for different factors and results, which are then verified through experiments.

II. CONFIGURATION OF CML COIL

There are two main methods for focusing the SV waves: one is to achieve the direction focusing of the beam by changing the spacing of the coil, and another is to realize the phase focusing of the SV waves by changing the spacing continuously. However, coherency for all the SV waves is not guaranteed with the beam focusing method [20, 21]. For the point focusing method of the SV waves, CML coil is used to achieve phase focusing at a certain point. In the design process of the PFSV-EMAT, since the amplitude directivity has a sharp peak at an angle of 30 °, it is necessary to properly set the position of the concentric line source (CLS) to ensure that each CLS's radiation angle is around 30 °, thereby ensuring that the SV wave has the largest signal amplitude at the focal point position and the phase is consistent at the same time.

Fig. 1(a) shows the 3D configuration of the PFSV-EMAT. The permanent magnet above the coil and aluminum specimen to provide the bias magnetic field for the Lorentz force generation. The top view of the CML coil is shown and the coil with changing spaces can be used to generate eddy currents in the specimen. The excitation current is a burst wave and the expression of the excitation burst current for the EMAT coil is

$$i(t) = I_c e^{-\alpha(t-\tau)^2} \cos[2\pi f(t-\tau)+\theta], \quad (1)$$

where I_c is the amplitude of the signal, α is the bandwidth factor, τ is the arrival time, f is the central frequency, and θ is the phase delay. Both the permanent magnet and the specimen are cylindrical in shape and are concentric with the coil, with the focal point on their symmetry axis. This transducer structure effectively focuses the generated SV waves to the focal position.

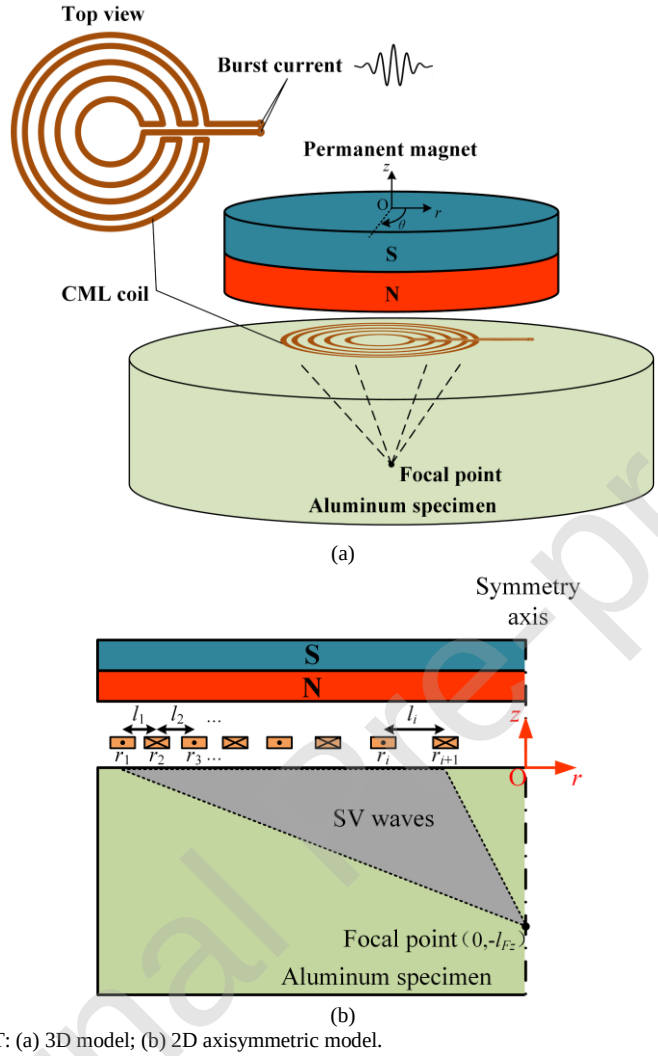

Fig. 1 Configuration of the PFSV-EMAT: (a) 3D model; (b) 2D axisymmetric model.

As observed in Fig. 1(a), the 3D structure of the transducer can be simplified to a two-dimensional axisymmetric structure, as shown in Fig. 1(b). According to the coordinate system definition in the figure, the coordinates of CLSs are (r_1, 0), (r_2, 0), ..., (r_i, 0), and the coil spacing is l_1, l_2, ..., l_i. the spacing between the coils generally satisfies the following formula

$$r_i - r_{i+1} = \frac{c}{2f} = \frac{\lambda}{2}, \quad (2)$$

where λ is the wavelength of the SV wave, c is the shear wave velocity, f is the frequency. The focal point locates on the symmetry axis and its distance from the origin is l_{Fz}.

III. Theory and Simulation

The generation and propagation of SV waves can generally be described by electromagnetic fields and ultrasonic fields. Ultrasonic waves are a kind of elastic wave generated by induced eddy currents in a conductor that propagates through the conductor due to the Lorentz force. The dynamic magnetic field equation of pulsed eddy current is

$$\frac{1}{\mu}\nabla^2 \boldsymbol{A} + \frac{1}{S}\iint_s \sigma \frac{\partial \boldsymbol{A}}{\partial t} \mathrm{d}s = \sigma \frac{\partial \boldsymbol{A}}{\partial t} - \frac{\boldsymbol{i}}{S}, \quad (3)$$

where $\boldsymbol{A}$ is the magnetic vector potential; σ is the conductivity; $\boldsymbol{i}$ is the total current; S is the cross-sectional area of the coil conductor. The induced eddy current density is

$$\boldsymbol{J}_{\mathrm{e}} = -\sigma \frac{\partial \boldsymbol{A}}{\partial t} \tag{4}$$

Then the Lorentz force $\boldsymbol{F}$ generated by the eddy current under the applied bias magnetic field is

$$\boldsymbol{F}_{\mathrm{v}} = \boldsymbol{J}_{\mathrm{e}} \times \left(\boldsymbol{B}_{\mathrm{d}} + \boldsymbol{B}_{\mathrm{s}} \right), \tag{5}$$

where $\boldsymbol{B}_{\mathrm{d}}$ is the dynamic magnet flux density; $\boldsymbol{B}_{\mathrm{s}}$ is the static magnetic flux density of the permanent magnet. It is well known that Lorentz force as a coupling factor plays an important role in the interaction of physical fields because the periodic Lorentz forces produce elastic waves propagating in a sample in a certain direction. The wave equation is equal to the Navier's equation of the elastic wave which can be expressed as

$$\left(\lambda + \mu \right) \nabla \nabla \cdot \boldsymbol{u} = \rho \frac{\partial^2 \boldsymbol{u}}{\partial t^2} - \mu \nabla^2 \boldsymbol{u} - \boldsymbol{F}_{\mathrm{v}} \tag{6}$$

where $\boldsymbol{u}$ is the displacement vector; $\boldsymbol{F}$ is the calculated Lorenz force in the electromagnetic field model; λ and μ are the Lame's constants of the material. It can be seen from the equation that the displacement of the specimen changes with time under the Lorentz force, which describes the propagation process of the elastic wave. The material parameters are shown in Table I.

TABLE I
MATERIAL PARAMETERS OF THE SPECIMEN

Parameters	Value
Specimen Lame's constants κ (GPa)	58
Specimen Lame's constants G (GPa)	29
Specimen mass density (kg/m^3)	2832
Specimen conductivity (S/m)	3.65×10^7
Magnet relative permeability	400
Magnet coercive force (MA/m)	0.9

The FEM simulation is used to calculate the propagation process of SV waves. As a particular case, the parameters are selected as follows. The coil width w is 0.2 mm, the lift-off distance h_l is 0.5 mm, the excitation current amplitude I_c is 50 A, the bandwidth factor α is 3×10^{11} s^{-2}, the line source number n is 10, the drive frequency f is 4 MHz, and the focal depth l_{Fz} is 30 mm. For the coil design, the coordinates and spacings for CLSs are shown in Fig. 2. It can be seen that as the CLS approaches the focal point, the spacing of the coil increases non-linearly.

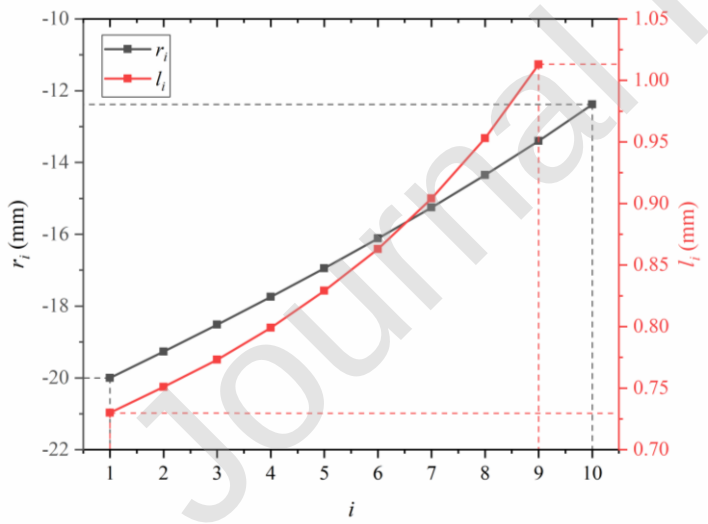

Fig. 2 Variation of the CLSs position and spacing of the PFSV-EMATs.

Simulation result that under certain conditions is shown in Fig. 3. It can be observed that the focal area does not locate on the symmetry axis according to the preset focus position [26], but the wave focusing can still be successfully achieved. A contour of 50% peak value of the displacement field is selected as the boundary of the effective focal area. As can be seen from the figure, the focal area is approximately an elliptical shape and has an oblique angle concerning the coordinate axis. Figs. 4(a, b) show the displacement distribution along Z-axis and R-axis. To determine the dimensions of the focal area, the r-z axis is rotated to the R-Z axis, where the diameter of the ellipse in the Z-axis is defined as the effective focal length L_{fd} and the R axis is defined as the

effective focal width W_{fd}. In addition, the elliptical center of the effective focal area is defined as the origin of the new coordinate system.

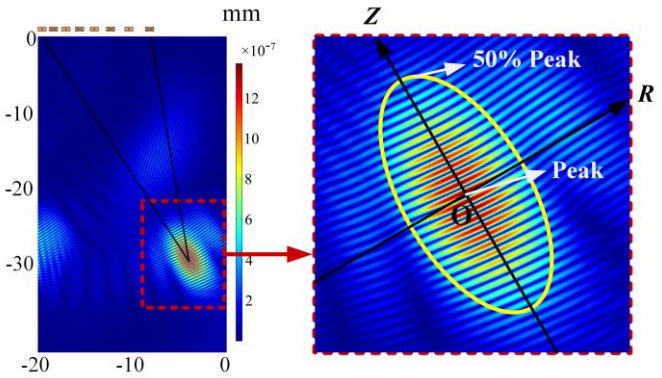

Fig. 3 Displacement field distribution of the PFSV-EMAT.

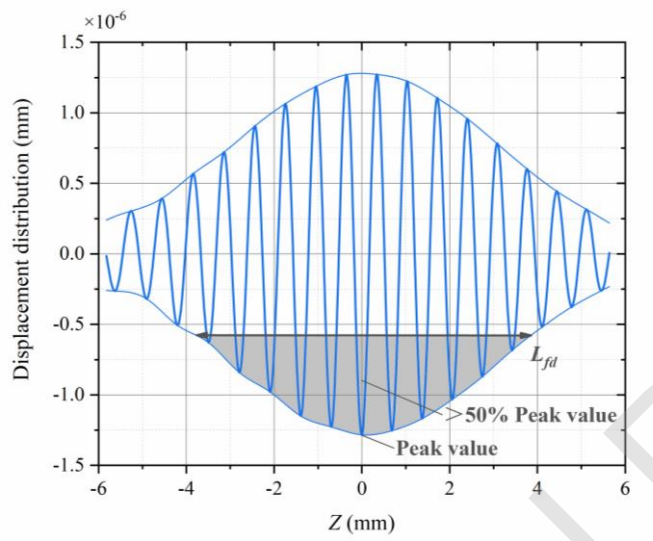

(a)

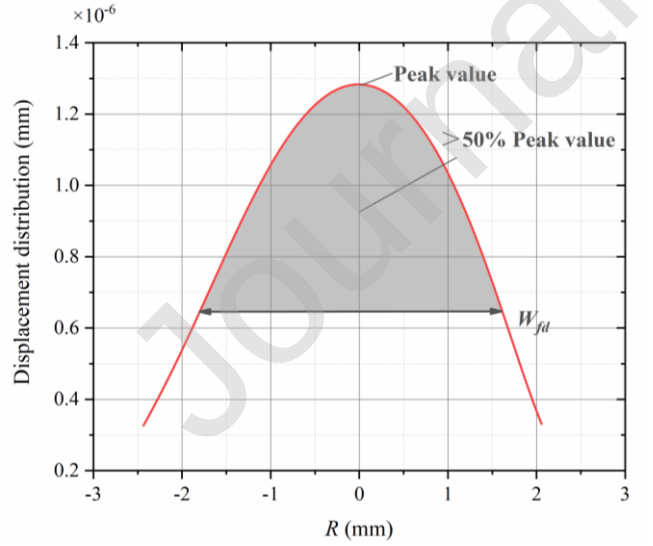

(b)

Fig. 4 Displacement distribution along (a) *Z*-axis; (b) *R*-axis.

IV. ORTHOGONAL TEST

A. Test Design

Orthogonal test design refers to a design method that studies multi-factors and multi-levels. Based on the orthogonality, some representative points are selected from the comprehensive test, and these representative points were uniformly dispersed and neatly comparable. [25] The orthogonal table is used as the main tool of the orthogonal test, and the choice depends on the number and level of factors in the test, and then the representative points are selected from the comprehensive test. This method of replacing large-scale tests with few tests will greatly improve the efficiency of scientific analysis. [27]. Therefore, as an effective multi-factor experimental design method, the orthogonal test method is chosen in this paper to analyze the focusing performance for PFSV-EMAT with different structures.

According to the calculation method of the signal-to-noise ratio of the EMAT's received signal, it can be found that a total of thirteen parameters affect the transducer's focusing performance [28]. Considering the possible coupling relationship between various parameters, such as magnet length, current frequency and focal length, nine independent parameters are determined: coil width w, lift-off distance h_l, excitation current amplitude I_c, bandwidth factor α, CLS number n, remanence magnetism of the permanent magnet B_r, coil aperture angle θ, focal depth l_{Fz}, and drive frequency f. Among them, B_r= 1.2 T and θ=360 ° are fixed as constants. An Independent study is performed because changes in f and l_{Fz} will change the spacing of the CLSs. Therefore, five factors w, h_l, I_c, α and n are finally selected as influence factors, f=4 MHz and l_{Fz} =50 mm are then fixed in the orthogonal test. The level for each factor is shown as follows. The levels of w are 0.2, 0.4, 0.6 and 0.8 mm; The levels of h_l are 0.5, 1, 1.5 and 2 mm; The levels of I_c are 50, 100, 150 and 200 A; The levels of α are 3×10^{11}, 5×10^{11}, 7×10^{11} and 9×10^{11} s^{-2}; The levels of n are 4, 6, 8 and 10. Therefore, for these five factors and four levels orthogonal test, the $L_{16}(4^5)$ orthogonal table is selected.

For the results, signal intensity M is always the most concerning focusing performance of a PFSV-EMAT, so the peak displacement value at the focal point is defined as M as one of the test results. Moreover, the size of the focal area should also be studied, as its size is related to the accuracy of defect detection. The smaller the focal area is, the more accurate the identification of defects is and the higher the resolution of the imaging is. Therefore, effective focal length L_{fd} and width W_{fd} are selected as the other two test results. Test results are shown in Table II.

TABLE II
RESULTS FOR THE ORTHOGONAL TEST

Test No.	Factors					Results		
	A	B	C	D	E	M ($\times10^{-7}$)	L_{fd}	W_{fd}
	w	h_l	I_c	α	n			
	mm	mm	A	$\times10^{11}$ s^{-2}	1	mm	mm	mm
1	0.2	0.5	50	3	4	2.3	7.19	8.79
2	0.2	1	100	5	6	1.83	7.12	6.13
3	0.2	1.5	150	7	8	1.2	7.3	4.19
4	0.2	2	200	9	10	0.68	7.59	3.31
5	0.4	0.5	100	7	10	14.3	7.46	3.18
6	0.4	1	50	9	8	2.02	7.45	4.4
7	0.4	1.5	200	3	6	2.82	7.61	5.78
8	0.4	2	150	5	4	0.48	6.68	10.9
9	0.6	0.5	150	9	6	17.8	7.7	6.56
10	0.6	1	200	7	4	6.39	7.21	10.62
11	0.6	1.5	50	5	10	1.47	6.97	3.24
12	0.6	2	100	3	8	0.96	7.47	4.16
13	0.8	0.5	200	5	8	43.72	6.93	4.12
14	0.8	1	150	3	10	15.74	7.49	3.29
15	0.8	1.5	100	9	4	1.37	8.07	11.02
16	0.8	2	50	7	6	0.39	7.07	6.17

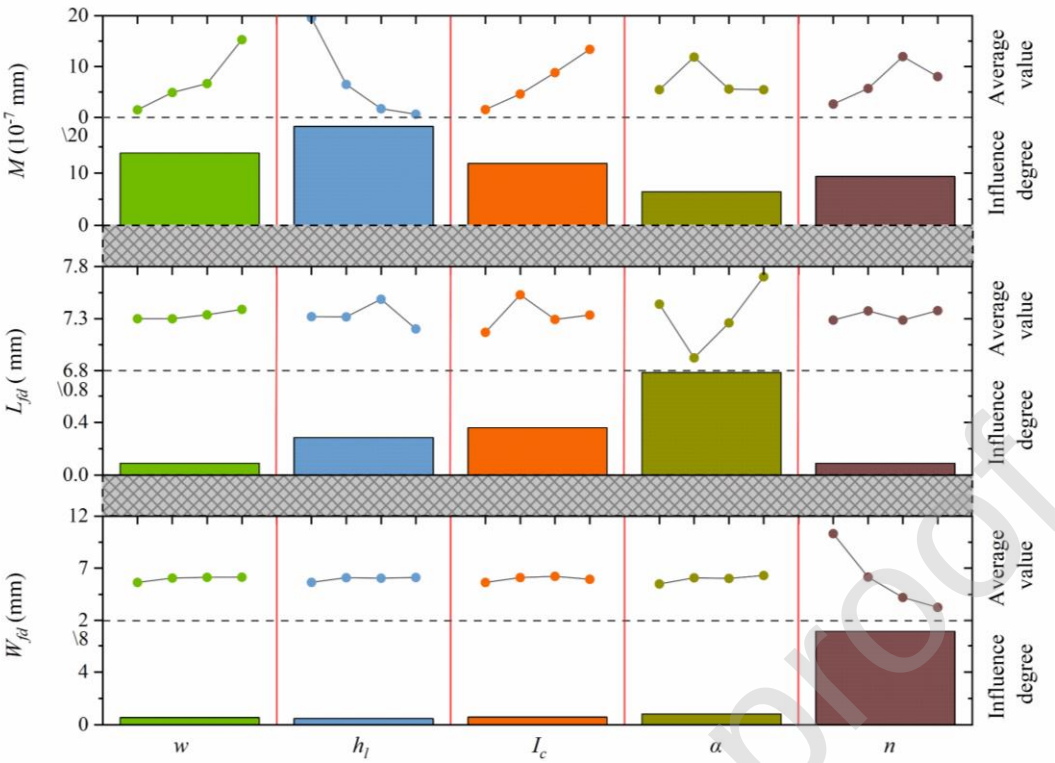

Fig. 5 Range analysis results for the orthogonal test, the column height represents the average value of each level and influence degree for each factor.

B. *Range Analysis*

Range analysis of the orthogonal method is required to obtain the influence degree of five factors on test results. In the calculation of the range analysis, the average value k_{ZN} and the influence degree T_Z are shown

$$k_{ZN} = \frac{1}{m}\sum_{i=1}^{n} y_{Zi}\,, \tag{7}$$

$$T_Z = R_{\max Z} - R_{\min Z}\,, \tag{8}$$

where i is the test number; Z represents the factor; y is the test result, which is the signal intensity; n=16; m=4; N is the level number. $R_{\max Z}=\max\{k_{Z1}, k_{Z2}, k_{Z3}, k_{Z4}\}$, $R_{\min Z}=\min\{k_{Z1}, k_{Z2}, k_{Z3}, k_{Z4}\}$. In the range analysis, the average value k_{ZN} when N=1, 2, 3, 4 describes the effect of the factor Z on the test result M. Moreover, the influence degree T_Z represents how large the impact of factor Z is. Using the analysis method above, the range analysis result with different k_{ZN} and T_Z are shown in Table III.

Fig. 5 shows the average value and influence degree of each factor on different results. It can be found that the factor that has the greatest effect on the signal intensity M is the lift-off distance h_l, followed by the coil width w, the excitation current amplitude I_c, the CLS number n, while the influence of the bandwidth coefficient α is the smallest. It is observed that the decrease in h_l will increase M, and the increase in w and I_c will increase M. For n and α, $M_{n=8}$ and $M_{\alpha=5E11}$ have the largest signal intensity.

For effective focal length L_{fd}, α has the largest effect on it, and I_c, h_l follow in order, while w and n have a relatively smaller influence on L_{fd}. In Fig. 5, it shows that when $\alpha=5\times10^{11}$ s^{-2}, I_c=50 A and h_l=2 mm, L_{fd} has the smallest value. In addition, for effective focal width W_{fd}, n has the largest effect, and W_{fd} decreases with the increase of n. The other four factors share nearly the same influence level, and these factors are not sensitive to changes in W_{fd}.

TABLE III
RANGE ANALYSIS FOR ORTHOGONAL TEST RESULTS

Results	Level	Factors				
		A	B	C	D	E
		w	h_l	I_c	α	n
M (10^{-7}mm)	1	1.5025	19.53	1.545	5.455	2.635
	2	4.905	6.495	4.615	11.875	5.71
	3	6.655	1.715	8.805	5.57	11.975
	4	15.305	0.6275	13.4025	5.4675	8.0475
	T_{XI}	13.8025	18.9025	11.8575	6.42	9.34
L_{fd} (mm)	1	7.3	7.32	7.17	7.44	7.2875
	2	7.3	7.3175	7.53	6.925	7.375
	3	7.3375	7.4875	7.2925	7.26	7.2875

	4	7.39	7.2025	7.335	7.7025	7.3775
	T_{X2}	0.09	0.285	0.36	0.7775	0.09
W_{fd} (mm)	1	5.65	5.6625	5.65	5.505	10.3325
	2	6.065	6.11	6.1225	6.0975	6.16
	3	6.145	6.0575	6.235	6.04	4.2175
	4	6.15	6.135	5.9575	6.3225	3.255
	T_{X3}	0.545	0.4725	0.585	0.8175	7.0775

C. *Effect of Frequency and Focal Depth*

Since the change in frequency f and focal depth l_{Fz} causes changes in the coil structure, independent research on these two factors is required. In the study, levels for five factors in the orthogonal test are fixed as w is 0.2 mm, h_l is 0.5 mm, I_c is 50 A, α is 3×10^{11} s^{-2}, and n is 10. Besides, focal depth l_{Fz} is fixed to 50 mm when investigating the effect of frequency f. Fig. 6 shows the effect of f on M, L_{fd}, and W_{fd}. With the increase of f, the test results M, L_{fd}, and W_{fd} decrease at the same time. When study effect of focal depth l_{Fz}, f is fixed to 4 MHz and Fig. 7 shows the simulation results that the increase in l_{Fz} results in the decrease in M and W_{fd}, but L_{fd} increases here.

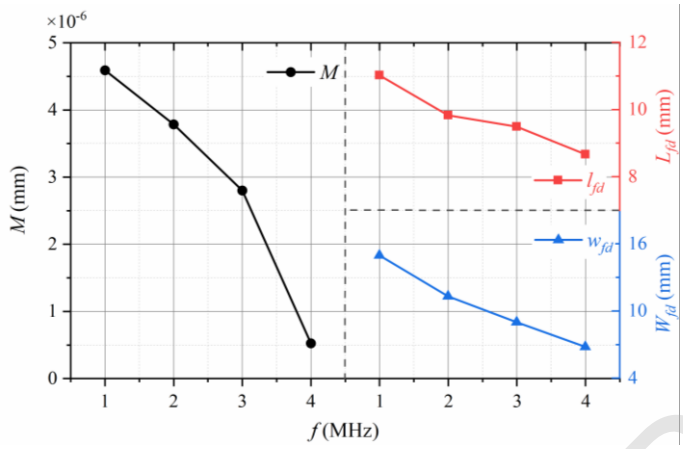

Fig. 6 The effect of the drive frequency f on the signal intensity M, effective focal length L_{fd}, and width W_{fd}.

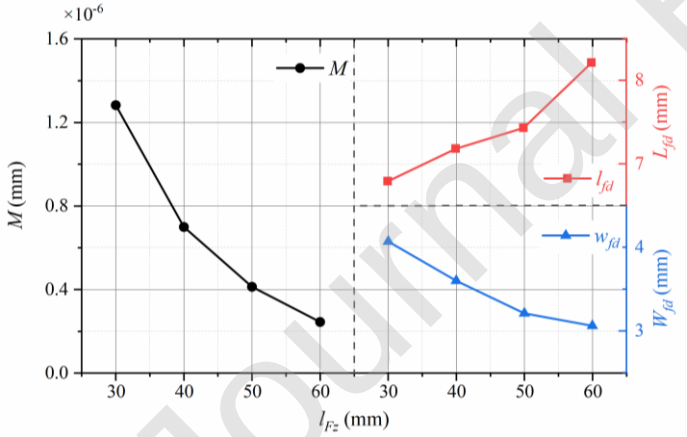

Fig. 7 The effect of the focal depth l_{Fz} on the signal intensity M, effective focal length L_{fd}, and width W_{fd}.

D. *Optimal Design*

To achieve the best PFSV-EMAT focusing performance, it is necessary to select a suitable combination of parameters to achieve high focal intensity and small focal area. From the range analysis, the levels of different factors can be determined when only considering the signal intensity M. The levels are selected as w=0.8 mm, h_l=0.5 mm, I_c=200 A, $\alpha=5\times10^{11}$ s^{-2}, n=8, f=4 MHz and l_{Fz}=50 mm. When considering focal area dimensions, such as effective focal length L_{fd}, α should be 5×10^{11} s^{-2} as the most influential factor. For W_{fd}, it is shown in Fig. 5 that n should be 10 to achieve a smaller W_{fd}. Therefore, to achieve better-focusing performance without changing the coil structure, the selection of parameters is finally determined as w=0.8 mm, h_l=0.5 mm, I_c=200 A, $\alpha=5\times10^{11}$ s^{-2}, n=10, f=4 MHz and l_{Fz}=50 mm.

V. EXPERIMENTS

The focusing performance of PFSV-EMAT is analyzed by the orthogonal method above to investigate its characteristics under different conditions. The experiments verify the validity of the simulation results. PFSV-EMAT is utilized in the experiments as the transmitting source, and bulk wave (BW) EMAT is used to receive the focusing signal. The schematic diagram of the experimental setup is shown in Fig. 8. PFSV-EMAT is placed above the aluminum specimen, and BW-EMAT is set at the focal point of the transmitter as the signal receiver. Due to the low energy conversion efficiency of EMAT, to obtain the maximum output power of the excitation source, it is required to match the impedance of the load with the internal impedance of the excitation source, then matching impedance are utilized in the experiment to improve the accuracy and the efficiency of the EMAT. As the most important signal source, the signal generation and reception in the experiment need to be modulated and amplified before processing. Therefore, the RPR-4000 pulse generator/receiver is selected in the experiment. An oscilloscope is used to show the waveform output by the signal source.

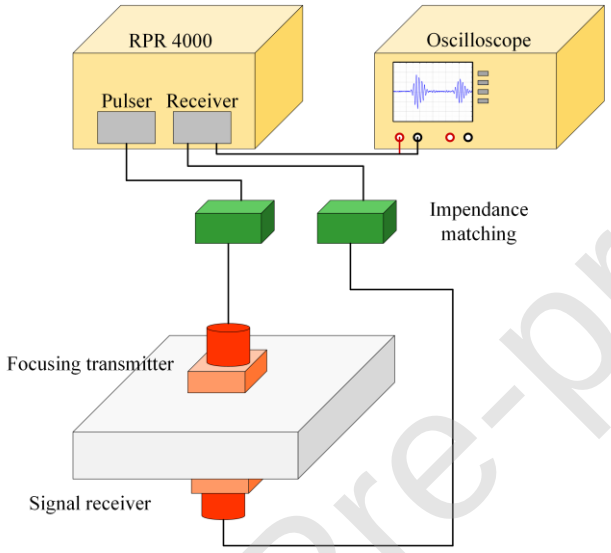

Fig. 8 Experimental configuration for measuring the signal of SV waves.

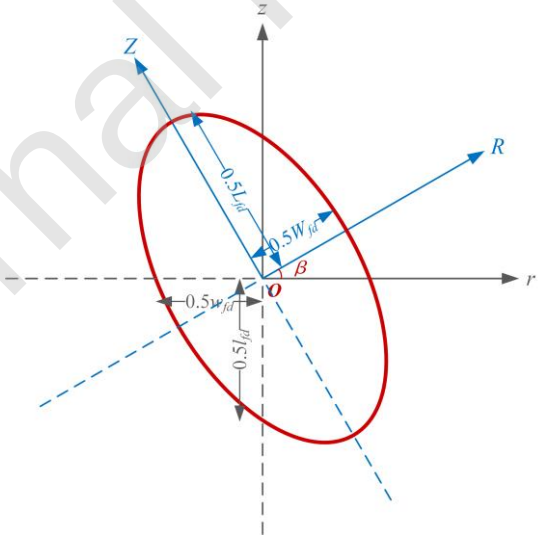

Fig. 9 Schematic diagram of the two coordinates of the focal area.

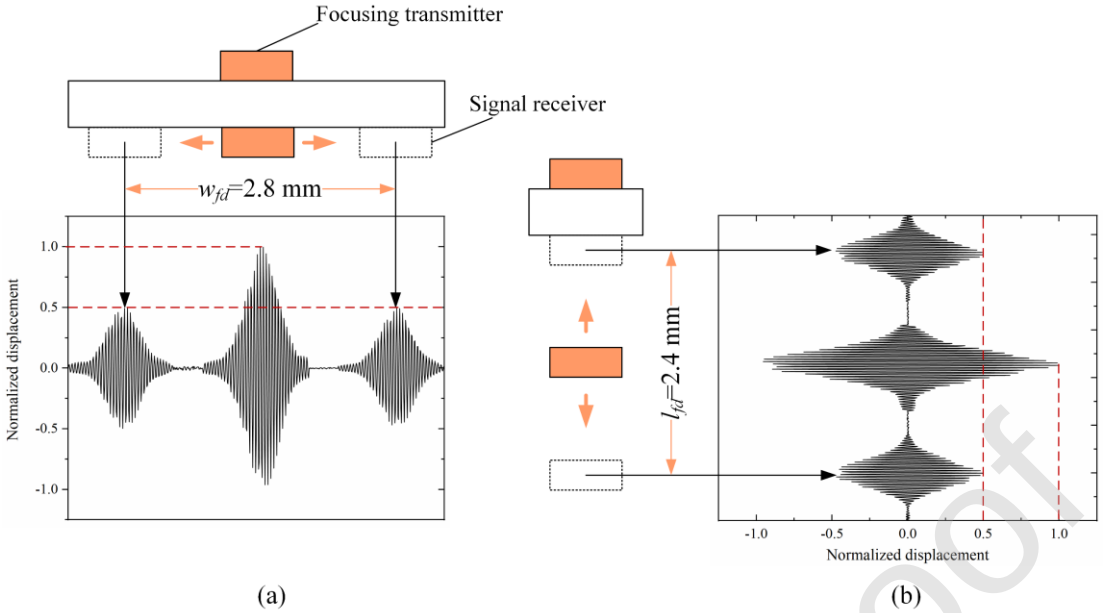

Fig. 10 Experiment method and results for PFSV-EMAY with optimized parameter combination.

It should be noted that although the signal amplitude can be measured since the dimensions of the focal area have a rotation angle relative to the *r*-*z* coordinate system, L_{fd} and W_{fd} cannot be directly obtained. However, in the experiment, the *r*-axis effective focal width w_{fd} of the focal area and the *z*-axis effective focal length l_{fd} can be measured. Fig. 9 shows that l_{fd} and L_{fd} are in a nonlinear proportional relationship, and w_{fd} and W_{fd} also satisfy the same proportional relationship. Therefore, the changes of L_{fd} and W_{fd} can be approximated to those of l_{fd} and w_{fd}. In the experiment, Fig. 10(a) shows that the horizontal position of the BW-EMAT can be changed to obtain w_{fd}. This method first measures the amplitude of the signal at the focal position, then moves the BW-EMAT horizontally, and records the transducer's positions when the signal is attenuated by 50%, thereby obtaining the effective focal width w_{fd}. The same procedure is equally applicable to the acquisition of l_{fd}, but the thickness of the sample needs to be constantly changed. The experimental results shown in Fig. 10 use the optimized parameter combination.

To compare the difference between the focusing performance of the PFSV-EMAT with optimized and non-optimized parameters, three unoptimized parameter combinations of orthogonal test numbers 1, 9, and 10 are selected and compared with the experimental results of the EMAT with optimized parameters. Fig. 11 shows the simulation and experimental results for four tests. It is observed that simulation and experiment are in good agreement, and the test with optimized parameters has the best focusing performance. The focusing intensity of the optimized transducer is 400% higher than the average level of the non-optimized transducer, the effective focal length is reduced by 15%, and the effective focal width is reduced by 57%.

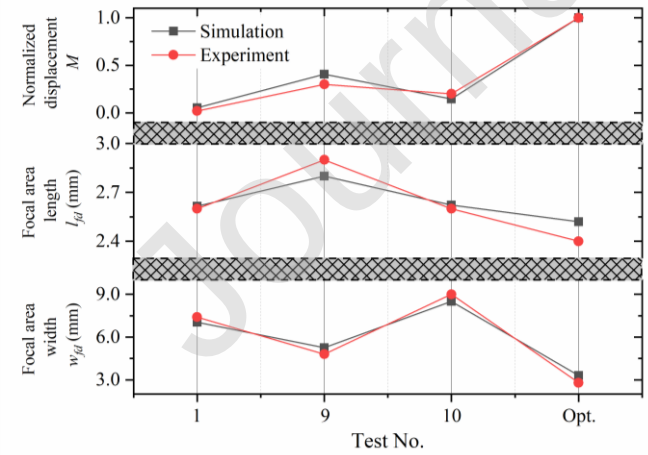

Fig. 11 Experiment and simulation results for test No. 1, 9, 10 and optimized one.

VI. Conclusion

In this work, FEM simulation and orthogonal test methods are used to study the effect of impact factors on the PFSV-EMAT's performance. Five factors are selected in the test to investigate the signal intensity and focal area dimensions of the transducer.

Range analysis is applied to compare the influence degree of each factor. In addition, drive frequency f and focal depth l_{Fz} are also studied individually.

Range analysis shows that the lift-off distance h_l has the largest effect on the signal intensity M, then the coil width w and the excitation current amplitude I_c follow in order. For effective focal length L_{fd}, bandwidth factor α has the largest effect, followed by I_c and h_l. Moreover, for effective focal width W_{fd}, n has the largest effect, and W_{fd} decreases with the increase of n. The other four factors are not sensitive to W_{fd}. It is also found that M, L_{fd}, and W_{fd} decrease with the increase of f, and the increase in l_{Fz} causes a decrease in M and W_{fd}, while L_{fd} increases. Considering the influence of different factors on different results, the optimal combination of parameters can be obtained. The effectiveness of the optimization method is verified by both simulation and experiment. Moreover, the experiments show that the focusing intensity of the optimized transducer is 400% higher than the average value of the non-optimized transducers, the effective focal length is reduced by 15%, and the effective focal width is reduced by 57%.

Author statement

Hongyu Sun: *Conceptualization, Methodology, Software, Writing - Original Draft* Songling Huang: *Supervision, Project administration* Qing Wang: *Visualization* Shen Wang: *Validation* Wei Zhao: *Resources, Formal analysis*

AUTHOR DECLARATION

We wish to confirm that there are no known conflicts of interest associated with this publication and there has been no significant financial support for this work that could have influenced its outcome.

We confirm that the manuscript has been read and approved by all named authors and that there are no other persons who satisfied the criteria for authorship but are not listed. We further confirm that the order of authors listed in the manuscript has been approved by all of us.

We confirm that we have given due consideration to the protection of intellectual property associated with this work and that there are no impediments to publication, including the timing of publication, with respect to intellectual property. In so doing we confirm that we have followed the regulations of our institutions concerning intellectual property.

We understand that the Corresponding Author is the sole contact for the Editorial process (including Editorial Manager and direct communications with the office). He is responsible for communicating with the other authors about progress, submissions of revisions and final approval of proofs. We confirm that we have provided a current, correct email address which is accessible by the Corresponding Author and which has been configured to accept email from huangsling@tsinghua.edu.cn

Declarations of interest: none

ACKNOWLEDGMENTS

This research was supported by the National Key R&D Program of China (Grant No. 2018YFF01012802), National Natural Science Foundation of China (NSFC) (No. 51677093) and National Natural Science Foundation of China (NSFC) (No. 51777100).

REFERENCES

[1] W. Ren, J. He, S. Dixon, K. Xu, "Enhancement of EMAT's efficiency by using silicon steel laminations back-plate," *Sens. Actuators, A.*, 274 (2018) 189-198.

[2] S. Wang, S. Huang, Y. Zhang, and W. Zhao, "Multiphysics Modeling of a Lorentz Force-Based Meander Coil Electromagnetic Acoustic Transducer via Steady-State and Transient Analyses," *IEEE Sens. J.*, 16, pp. 6641-6651, (2016).

[3] M. Hirao and H. Ogi, "An SH-wave EMAT technique for gas pipeline inspection," *NDT&E Int.*, 32, pp. 127-132, (1999).

[4] S. Huang, L. Peng, Q. Wang, S. Wang, and W. Zhao, "An Opening Profile Recognition Method for Magnetic Flux Leakage Signals of Defect," *IEEE T. Instrum. Meas.*, 68, pp. 2229-2236, (2019).

[5] C. B. Thring, Y. Fan and R. S. Edwards, "Multi-coil focused EMAT for characterisation of surface-breaking defects of arbitrary orientation," *NDT&E Int.*, 88, pp. 1-7, (2017).

[6] J. Silva, M. Wamzeller, P. Farias and J. Neto, "Development of Circuits for Excitation and Reception in Ultrasonic Transducers for Generation of Guided Waves in Hollow Cylinders for Fouling Detection," *IEEE Trans. Instrum. Meas.*, vol. 57, no. 6, pp. 1149-1153, 2008.

[7] H. Sun, S. Wang, S. Huang, Q. Wang, and W. Zhao, "Point-Focusing of Shear-Horizontal Wave Using Fan-Shaped Periodic Permanent Magnet Focusing Coils EMAT for Plate Inspection," *IEEE Sens. J.*, 19, pp. 4393-4404, (2019).

[8] Sun H, Huang S, Wang Q, Wang S, Zhao W, "Improvement of unidirectional focusing periodic permanent magnet shear-horizontal wave electromagnetic acoustic transducer by oblique bias magnetic field," *Sensors and Actuators: A. Physical.* 290, 36-47, 2019.

[9] Songling Huang, Hongyu Sun, Qing Wang, Shen Wang, Wei Zhao. "Unidirectional Focusing of Horizontally Polarized Shear Elastic Waves Electromagnetic

Acoustic Transducers for Plate Inspection," *J. Appl. Phys.*, vol. 125, no. 17, 2019.
[10] S. Legendre, D. Massicotte, J. Goyette, et al, "Wavelet-transform-based method of analysis for Lamb-wave ultrasonic NDE signals," *IEEE Trans. Instrum. Meas.*, vol. 49, no. 3, pp. 524-530, 2000.
[11] H. M. Seung, C. I. Park, and Y. Y. Kim, "An omnidirectional shear-horizontal guided wave EMAT for a metallic plate," *Ultrasonics*, vol. 69, pp.58–66, 2016.
[12] Y. Zhang, S. Huang, S. Wang, et al, "Direction-controllable electromagnetic acoustic transducer for SH waves in steel plate based on magnetostriction," *Prog. Electromagn. Res. Symp.*, vol. 50, pp.151-160, 2016.
[13] Nurmalia, N. Nakamura, H. Ogi, and M. Hirao, "Detection of shear horizontal guided waves propagating in aluminum plate with thinning region," *Jpn. J. Appl. Phys.*, vol. 50, no. 7S, pp.07HC17, 2011.
[14] N. Lunn, S. Dixon, and M. D. G. Potter, "High temperature EMAT design for scanning or fixed point operation on magnetite coated steel," *NDT&E Int.*, vol. 89, pp. 74–80, Jul. 2017.
[15] R. Ribichini, F. Cegla, P. B. Nagy, and P. Cawley, "Study and comparison of different EMAT configurations for SH wave inspection," *IEEE Trans. Sonics Ultrason.*, vol. 58, no. 12, pp. 2571–2581, 2011.
[16] Lee, J. K., H. W. Kim, and Y. Y. Kim, "Omnidirectional lamb waves by axisymmetrically configured magnetostrictive patch transducer," *IEEE Trans. Sonics Ultrason.*, vol. 60, pp.1928–1934, 2013.
[17] X. Song, G. Qiu, "Optimization of a focusable and rotatable shear-wave periodic permanent magnet electromagnetic acoustic transducers for plates inspection," *Sensors*, vol. 17, no. 12, pp.2722, 2017.
[18] G. Waag, L. Hoff, P. Norli, "Air-coupled ultrasonic through-transmission thickness measurements of steel plates," *Ultrasonics*, **56**, 332(2015)
[19] S. F. Wang, Y. Fan, W. C. Tian, et al., "An air-coupled capacitive micromachined ultrasound transducer for noncontact nondestructive evaluation," *IEEE Sensors*, 1464(2007)
[20] H. Ogi, M. Hirao, T. Ohtani, "Line-focusing of ultrasonic SV wave by electromagnetic acoustic transducer," *J. Acoust. Soc. Am.* vol. 103, pp. 2411-2415, 1998.
[21] H. Ogi, M. Hirao, T. Ohtani, "Line-focusing electromagnetic acoustic transducers for the detection of slit defects," *IEEE Trans. Ultrason Ferr.* vol. 46, pp. 341, 1999.
[22] Takishita T, Ashida K, Nakamura N, et al., "Development of shear-vertical-wave point-focusing electromagnetic acoustic transducer," *Jpn. J. Appl. Phys.* vol. 54, pp. 07HC04, 2015.
[23] C. Pei, S. Zhao, P. Xiao, and Z. Chen, "A modified meander-line-coil EMAT design for signal amplitude enhancement," *Sens. Actuators A, Phys.*, vol. 247, pp. 539–546, Aug. 2016.
[24] L. Kang, S. Wang, T. Jiang, and G. Zhai, "Optimal design of Lamb wave electromagnetic acoustic transducers for improving their excitation performance," *Jpn. J. Appl. Phys.*, vol. 50, no. 7, p. 07HD01, 2011.
[25] X. Jia, Q. Ouyang. "Optimal Design of Point-focusing Shear Vertical Wave Electromagnetic Ultrasonic Transducers based on Orthogonal Test Method," *IEEE Sens. J.* vol. 18, pp. 8064-8073, 2018
[26] J. Isla and F. Cegla, "EMAT phased array: A feasibility study of surface crack detection," *Ultrasonics*, vol. 78, pp. 1–9, Jul. 2017.
[27] J. Peng *et al.*, "Orthogonal test design for optimization of supercritical fluid extraction of daphnoretin, 7-methoxy-daphnoretin and 1,5-diphenyl-1-pentanone from Stellera chamaejasme L. and subsequent isolation by high-speed counter-current chromatography," *J. Chromatogr. A*, vol. 1135, pp. 151–157, 2006.
[28] D. MacLauchlan et al., "Recent advancements in the application of Emats to NDE," in Proc. 16th WCNDT, Montreal, QC, Canada, pp. 1154–1161, 2004.

Author Biography

Hongyu Sun received the B.S degree from the Department of Renewable Energy, North China Electric Power University, Beijing, China, in 2015, and the master's degree from the department of Electrical and Electronic Engineering, North China Electric Power University, Beijing, China, in 2018.

He is currently pursuing the Ph.D. degree within the Department of Electrical Engineering, Tsinghua University. His major research interests include nondestructive evaluation, acoustic metamaterials, plasma physics and artificial intelligence.

Songling Huang received the bachelor's degree in automatic control engineering from Southeast University, Nanjing, China, in 1991, and the Ph.D. degree in nuclear application technology from Tsinghua University, Beijing, China, in 2001.

He is currently a Professor within the Department of Electrical Engineering, Tsinghua University. His research interests include nondestructive evaluation and instrument techniques.

Qing Wang received the B.Eng. in electronic instrument and measurement technique from Beihang University, Beijing, China, in 1995, the M.Sc. degree in advanced manufacturing and materials from the University of Hull, Hull, U.K., in 1998, and the Ph.D. degree in manufacturing management from De Montfort University, Leicester, U.K., in 2001.

She is currently an Associate Professor in the School of Engineering and Computing Sciences, Durham University, Durham, U.K. Her research interests include electronic instruments and measurement, computer simulation, and advanced manufacturing technology.

Shen Wang received the bachelor's and Ph.D. degrees in electrical engineering from Tsinghua University, Beijing, China, in 2002 and 2008, respectively.

He is currently a Research Assistant within the Department of Electrical Engineering, Tsinghua University. His research interests include nondestructive testing and evaluation, and virtual instrumentation.

Wei Zhao received the bachelor's degree in electrical engineering from Tsinghua University, Beijing, China, in 1982, and the Ph.D. degree from the Moscow Power Engineering Institute Technical University, Moscow, Russia, in 1991.

He is currently a Professor within the Department of Electrical Engineering, Tsinghua University. His research interests include

modern electromagnetic measurement and instrument techniques.